Supplement of Biogeosciences, 23, 5961–5982, 2026
https://doi.org/10.5194/bg-23-5961-2026-supplement

Biogeosciences Open Access EGU

Supplement of

Buoyancy and polarity driven accumulation of dissolved organic matter in the sea surface microlayer during a phytoplankton bloom

Jasper Zöbelein et al.

Correspondence to: Jasper Zöbelein (jasper.zoebelein@uni-oldenburg.de)

S1. Supplemental Data and Figures

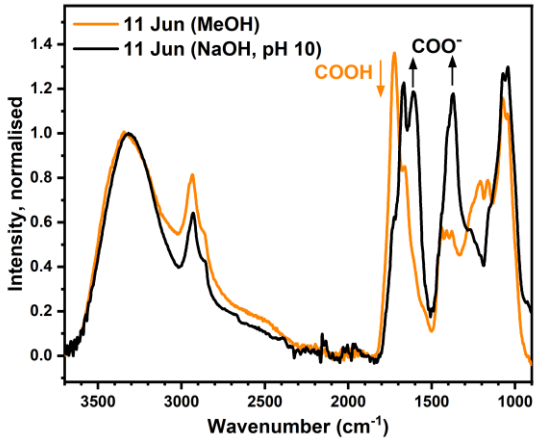

Fig. S1: FTIR spectra of DOM deposits on the ATR crystals from MeOH and NaOH (pH = 10) solution, respectively. For better comparison, the two spectra have been normalised with respect to the maximum of the broad OH/NH bad at 3300 cm^{-1}. As it is outlined in the main text, the very pronounced changes in the spectral signature indicates a high abundance of carboxyl/carboxylate functional groups.

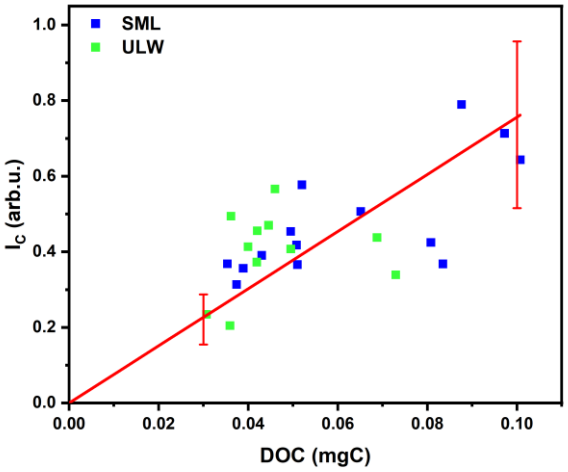

Fig. S2: Correlation between dissolved organic carbon (DOC, mg C in extract) versus integrated ATR-FTIR absorbance of carbon-containing functional groups (I_C; sum of all peak areas, except peaks related to O-H / N-H stretching). The solid line corresponds to a linear fit: I_C = (7.56 ± 0.44) ×DOC (with fixed intercept, r = 0.96, p < 0.0001). By using the ratio I_C/m as a mass balance correction factor (see main text), it is implicitly assumed that the scatter in the plot is mainly due to the limited reproducibility of the ATR-FTIR analysis and that the DOC measurement is reliable. The error bars indicate the ±30% (1σ standard deviation) uncertainty of

the FTIR measurements from the reference experiments using Triton-X 100. Considering that the experimental data points correspond to the mean of 3-7 individual measurements, the data points exhibit a higher scatter than expected from these reference measurements - presumably indicating the sample-to-sample variability of the DOM pool.

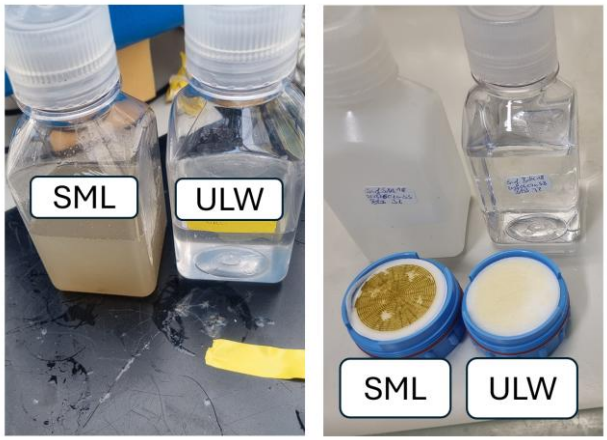

Fig S3: Left: unfiltered samples of sea surface microlayer (SML) and underlying water (ULW) during the post-bloom phase. Right: Filters of the same samples showing high amounts of particulate organic matter (POM) accumulating in the SML sample and being removed by filtration.

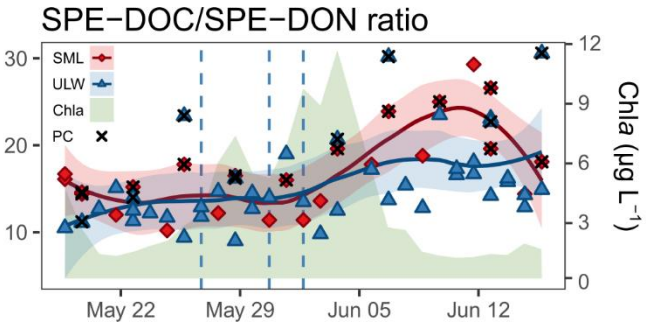

Fig S4: Solid-phase extractable dissolved organic carbon to solid phase extractable dissolved organic nitrogen (SPE-DOC/SPE-DON)-ratio. SML in red, ULW in blue; the green area indicates Chla development; dotted line indicates nutrient addition; black cross indicates poly carbonate (PC) filter, with glass fibre filter (GFF) as default.

Table S1: Selected peak positions with constraining FWHM for spectral decomposition of the ATR-FTIR spectra.

peak no.	peak center (cm^{-1})	constrained FWHM range (cm^{-1})
1	1065	50-200
2	1165	50-100
3	1215	50-100
4	1310	50-300
5	1390	50-200
6	1445	50-200
7	1665	50-200
8	1730	50-200
9	2510	30-500
10	2930	50-500
11	2940	50-100
12	3185	50-500
13	3390	30-500

Table S2: Assignment for the 13 spectrally decomposed ATR-FTIR peaks for SML and ULW DOM samples (Socrates 2001 and listed references).

$\tilde{\nu}$ (cm^{-1})	designation in main text	assignment	typical compound	references
3390, 3185, 2930	**O-H / N-H**	O–H stretch with possible minor N–H "amide A" contribution	alcohols, phenols, amines	Laurson et al. 2020 Pärnpuu et al. 2022 Božič et al. 2018 Yan Ji et al. 2020 Minor et al. 2008
2940	**C-H**	aliphatic C–H stretches (CH_3/CH_2)	fatty acids, lipids/aliphatic, polysaccharides/carbo-hydrates	Rong Lu et al. 2005 Pärnpuu et al. 2022 Minor et al. 2008 Artz et al. 2008
2510	**O-H / N-H**	broad acid O–H envelope tail or aromatic ester	carboxylic acids, aromatic esters	Minor et al. 2008
1730	**C=O**	C=O stretch	carboxylic acids, esters	Artz et al. 2008 Minor et al. 2008

1665	**amide I**	amide I, C=C	proteinaceous compounds, unsaturated lipids	Yan Ji et al. 2020 Minor et al. 2008 Abdulla et. al. 2010
1445, 1390		C-H deformation, OH in- plane bending	aliphatic compounds	Artz et al. 2008 Abdulla et. al. 2010
1309		C–O stretch of aromatic ester/aryl–O or amide III band		Artz et al. 2008 Yan Ji et al. 2020
1215, 1165		C–O stretch, C-O-C	esters, ethers, secondary alcohols	Minor et al. 2008
1065	**C-O/C-O-C**	C–O stretch glycosidic C-O-C	polysaccharides/carbo-hydrates	Pärnpuu et al. 2022 Abdulla et.al 2010 Minor et al. 2008 Artz et al. 2008

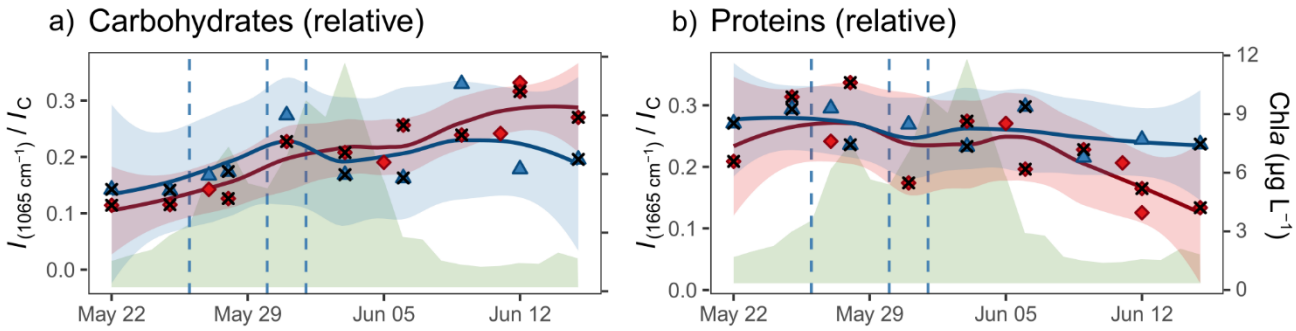

Fig. S5: The relative FTIR spectral intensity trend of the 1065 cm⁻¹ band characteristic of carbohydrate-like substances and the 1665 cm⁻¹ band characteristic of amide-I stretch vibration in protein-like substances, respectively. SML in red, ULW in blue; the green area indicates Chl*a* development; the dotted line indicates nutrient addition; the black cross indicates a polycarbonate filter, with GFF as default.

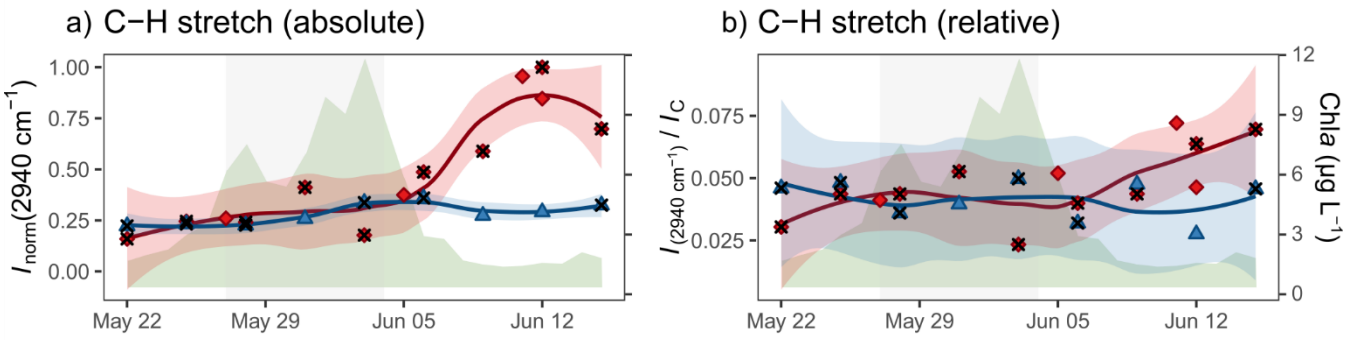

Fig. S6: The absolute and relative spectral intensity trend of the 2940 cm^{-1} band assigned to C-H stretch is highlighted for the SML (red symbols and LOESS trend line) and the ULW (blue symbol and trend line) in panels (a) and (b). The green area indicates Chl*a* development, dotted lines indicate nutrient additions, and black crosses indicate poly carbonate filter extracts, with GFF as default. I_C corresponds to the total integral of carbon-containing functional group peaks.

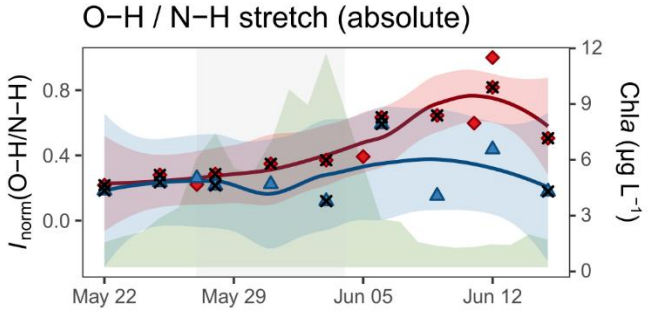

Fig. S7: The absolute intensity trend of the O-H / N-H vibrations (3390, 3185, 2930 and 2510 cm^{-1}) is highlighted for the SML (red symbols and LOESS trend line) and the ULW (blue symbol and trend line) in panel. The green area indicates Chl*a* development, dotted lines indicate nutrient additions, and black crosses indicate poly carbonate filter extracts, with GFF as default.

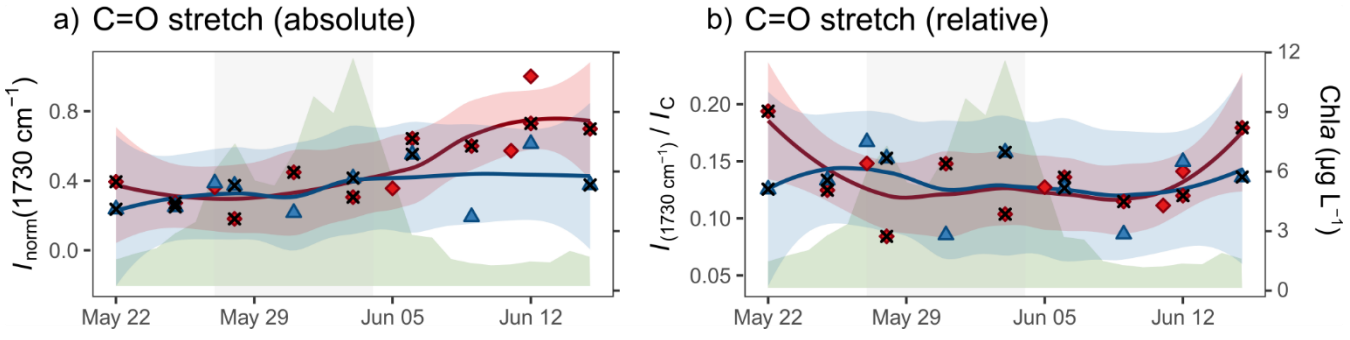

Fig S8: The absolute and relative spectral intensity trend of the 1730 cm^{-1} assigned to carboxylic acid is highlighted for the SML (red symbols and LOESS trend line) and the ULW (blue symbol and trend line) in panels (a) and (b), which is highlighted. The green area indicates Chl*a* development, dotted lines indicate nutrient additions, and black crosses indicate poly carbonate filter extracts, with GFF as default.

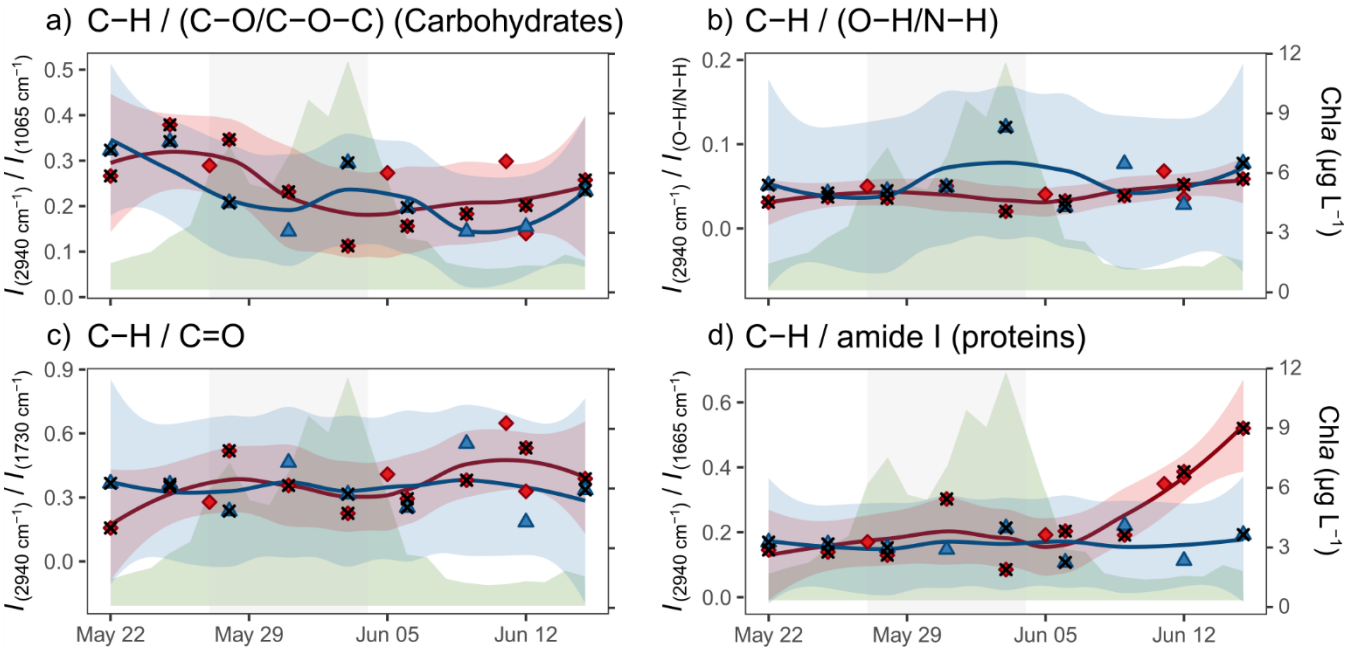

Fig S9: a): FTIR spectral ratio trends for a) Ratios C-H / (C-O / C-O-C) (1065 cm-1) , b) C-H / (O-H / N-H) (3390, 3185, 2930, 2510 cm-1), c) C-H / C=O (1730 cm-1) and d) C-H / amide I (1665 cm-1). SML in red, ULW in blue; the green area indicates Chla development; dotted line indicates nutrient addition; black cross indicates poly carbonate filter, with GFF as default.

Tab. S3: Dissolved organic matter (DOM) characteristics of mesocosm study samples during the three bloom phases as well as reference values for natural water samples.

Origin	Depth	H/C (w.a.)	O/C (w.a.)	I_{DEG}	MLB_{wL}	AI_{mod} (w.a.)	I_{bio}	I_{photo}	Carbo-hydrate-like (w.a. %)	Lipid-like (w.a. %)
pre-bloom	SML	1.20	0.46	0.52	5.87	0.29	0.54	0.36	0.33	0.07
	n=14	±0.01	±0.01	±0.05	±0.39	±0.01	±0.05	±0.02	±0.09	±0.03
	ULW	1.20	0.45	0.53	5.83	0.29	0.52	0.36	0.32	0.07
	n=24	±0.01	±0.01	±0.04	±0.37	±0.00	±0.05	±0.02	±0.10	±0.04
	t-test / p-value	0.63	0.91	0.69	0.76	0.5	0.46	0.65	0.68	0.8
bloom	SML	1.21	0.45	0.51	7.08	0.28	0.53	0.35	0.56	0.12
	n=15	±0.00	±0.01	±0.03	±0.42	±0.00	±0.02	±0.02	±0.10	±0.04
	ULW	1.20	0.46	0.52	6.60	0.29	0.53	0.34	0.51	0.08
	n=22	±0.01	±0.01	±0.04	±0.43	±0.01	±0.02	±0.02	±0.14	±0.02
	t-test / p-value	0.04 *	0.32	0.52	0.0017 **	0.24	0.56	0.65	0.23	0.0011 **
post-bloom	SML	1.22	0.46	0.48	8.83	0.27	0.57	0.31	1.06	0.14
	n=16	±0.01	±0.01	±0.05	±0.89	±0.01	±0.05	±0.02	±0.29	±0.03
	ULW	1.22	0.46	0.46	7.71	0.28	0.56	0.30	0.64	0.10
	n=26	±0.01	±0.01	±0.06	±0.51	±0.00	±0.07	±0.03	±0.26	±0.04
	t-test / p-value	0.17	0.76	0.39	<0.001 ***	0.072	0.66	0.44	<0.001 ***	0.005 **
[1]Mid-Bay	SML	1.44 ±0.41	0.295 ±0.20							
	ULW	1.50 ±0.40	0.332 ±0.22							
[2]Upper estuary	SML	1.23	0.46	0.21						
	ULW	1.22	0.45	0.20						
[2]Middle estuary	SML	1.25	0.47	0.23						
	ULW	1.23	0.47	0.20						
[2]Marine station	SML	1.27	0.48	0.21						
	ULW	1.25	0.49	0.17						
[3]North SW				0.63 ±0.01	11.9 ±0.8					
[4]North SW		1.26 ±0.01	0.40 ±0.03		12	0.28 ±0.02				
NEqPIW	n=6	1.26 ±0.00	0.46 ±0.00	0.84 ±0.01	4.69 ±0.12	0.23 ±0.00	0.02 ±0.01	0.27 ±0.02	0.14 ±0.02	0.02 ±0.12

Averages (± standard deviation) were calculated from experimental replicates

p-value significance: * (< 0.05), ** (< 0.01), and *** (< 0.001)

North SW North Sea seawater, *NEqPIW* North Pacific Equatorial Intermediate Water

[1]Burdette et al. (2022), June 2019. Quadrupole time-of-flight MS data (qToF-MS)

[2]Lechtenfeld et al. (2013), May 2009

[3]Waska and Banko-Kubis (2024), June 2020
[4]Amoako et al. (2025), October 2022

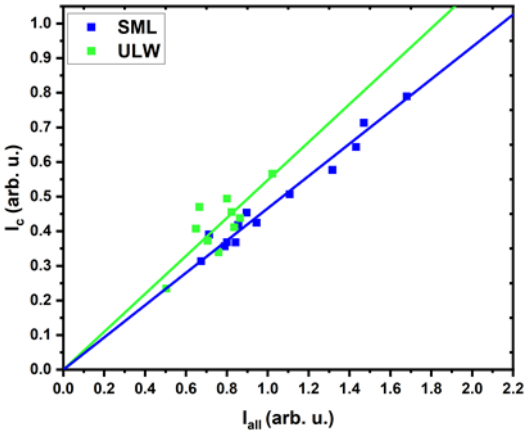

Fig. S10: Correlation between integrated ATR-FTIR total absorbance (I_{all}) versus integrated ATR-FTIR absorbance of carbon containing functional groups (I_C). The lines correspond to linear regressions with fixed intercept ($r > 0.99$) resulting in a ULW/SML slope ratio of 0.54/0.46 = 1.17. Interestingly, the I_C/I_{all} ratio turned out to be 17% higher in average for the ULW samples, possibly indicating a slight enrichment of OM rich of O-H and N-H groups in the SML.

S2. FTIR data evaluation

We evaluated the FTIR data using two complementary approaches. **1.)** ***Relative normalisation approach*****:** Here, we normalised the spectra to the integrated absorbance of the carbon-containing functional-groups, I_C. The resulting relative spectral trends have been shown in the Figs. S8, S9b, and S11b. This procedure enables us to evaluate how the contribution of an individual functional group changes relative to the overall carbon-related FTIR signal. The benefit of this approach is that sample-to-sample intensity variations as well as the overall trend in DOC mass do not matter. However, a drawback is that an apparent trend in the relative intensity of a particular band may in fact result from a substantial change in another band that also contributes to the overall spectral intensity I_C. 2.) ***DOC-based ATR-correction approach:*** Here, we applied a DOC-based correction to reduce ATR-related intensity fluctuations aiming to derive robust absolute signal intensity trends: $I_{corrected} = I_{raw} \times (V_{sample})^{-1} \times (I_C/m)^{-1}$. These corrected values are used in the main text to interpret changes in absolute functional-group abundance. Note that the normalisation with respect to V_{sample} is simply necessary to account for the variability in sample volumes used during the extraction process. More important is the factor $(I_C/m)^{-1}$ that rescales the overall intensity with respect to the independently measured DOC mass. Doing so, it is implicitly assumed that (i) I_C adequately reflect the total DOC content, so that compositional trends (despite the expected variability in the contributions of the functional groups) do not distort the overall intensity too much, and (ii) that the DOC measurement is in fact more reliable than our absolute I_C value (because of the expected ATR-related sample fluctuations).

To evaluate the robustness of the reported compositional trends, the following Figures S11 and S12 and Tables S4 and S5 show comparative results with different normalisation and data reduction procedures. Fig. S11 compares the *absolute* trends with (termed $I_{corrected}$ in Fig. S11) or without DOC-rescaling (termed I'_{raw}) . While the overall trends are unchanged, the scatter is somewhat reduced after DOC rescaling, which is more clearly visible in the protein data. Fig. S12 depicts the *relative* trends, either referenced to the integral over carbon-containing groups (I_C) or the total spectral intensity including the broad O-H / N-H band (I_{all}). Again, the trends stay the same (relative signal contribution increase for carbohydrate and decrease for the protein band, respectively). Finally, Tables S4 and S5 present a beginning-vs.-end comparison in terms of *absolute* and *relative* signal ratios. For this purpose, the first four (T1) and last five (T2) measurement points were averaged over the course of the mesocosm experiment. Although the absolute signal intensities fluctuate to some degree, the overall patterns represented by the end/beginning ratios (T2/T1 values) remain the same within error limits. In conclusion, regardless of how the spectra are processed, the reported trends are stable and reproducible.

For the final analysis, we chose I_C for both relative normalisation and DOC based correction rather than the integrated total absorbance of the whole spectrum (or total signal), I_{all} , for three main reasons: 1.) I_C shows a linear relationship with DOC (see Fig. S2; r = 0.96, p < 0.0001), suggesting that it is a suitable proxy for bulk carbon content and therefore an appropriate choice for reducing ATR-related scatter in our data. 2.) The alternative integral I_{all} is strongly influenced by the broad band resulting from OH/NH vibrations, adding up to about half of the total spectral intensity. As such, this broad band is particularly sensitive to residual water content in the samples. Therefore, including this band bears the risk of smearing out potential spectral trends related to OM. 3.) The necessary baseline correction of the FTIR spectra is more difficult for broad bands such that related systematic errors may become more prominent.

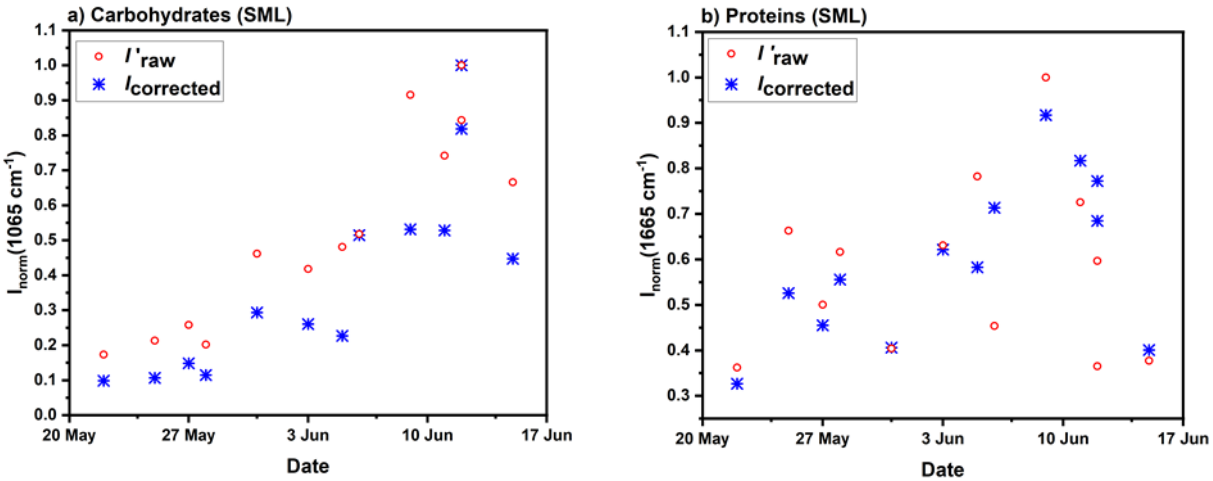

Fig. S11: Comparison of raw band integrals (I'_{raw} = I_{raw} / V_{sample}) and DOC-rescaled FTIR integrals ($I_{corrected}$ = I_{raw} . $(V_{sample})^{-1}$. $(I_C/m)^{-1}$) for the carbohydrate peak (a) and the protein peaks (b). Both datasets show the same overall temporal trend, with reduced scatter for the $I_{corrected}$ values.

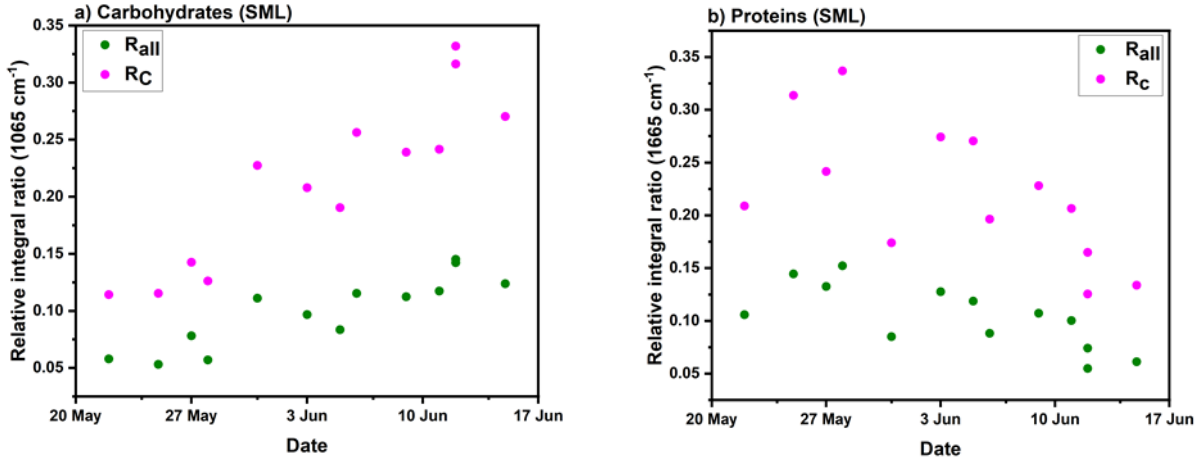

Fig. S12: Comparison of relative integral ratios $R_C = I_{raw} / I_C$ and $R_{all} = I_{raw} / I_{all}$ with respect to either the integral over carbon-containing groups (I_C) or the total spectral intensity including the broad OH/NH band (I_{all}), both for the carbohydrate peak (a) and the protein peak (b). Both datasets show the same overall temporal trend, with values about half because $I_{all} \approx 2 \times I_C$.

Table S4: Comparison of the mean FTIR integrals of the carbohydrate-associated peak in SML samples over the beginning (T1, 1s uncertainty, N = 4) and end phases (T2, 1s uncertainty, N = 5) of the mesocosm experiment. The I values refer to absolute, the R values to relative trends (see text).

	I'_{raw} / arb. u.	$I_{corrected}$ / arb. u.	$R_C = I / I_C$	$R_{all} = I / I_{all}$
T1 May 22 – May 28	0.21 ± 0.04	0.12 ± 0.02	0.12 ± 0.01	0.06 ± 0.01
T2 June 9 – June 15	0.83 ± 0.13	0.67 ± 0.23	0.28 ± 0.04	0.13 ± 0.01
T2 / T1	3.94 ± 0.91	5.67 ± 2.26	2.25 ± 0.42	2.08 ± 0.45

Table S5: Comparison of the mean FTIR integrals of the protein-associated peak in SML samples over the beginning (T1, 1s uncertainty, N = 4) and end phases (T2, 1s uncertainty, N = 5) of the mesocosm experiment. The I values refer to absolute, the R values to relative trends (see text).

	I'_{raw} / arb. u.	$I_{corrected}$ / arb. u.	$R_C = I / I_C$	$R_{all} = I / I_{all}$
T1 May 22 – May 28	0.54 ± 0.13	0.47 ± 0.10	0.28 ± 0.06	0.13 ± 0.02
T2 June 9 – June 15	0.61 ± 0.26	0.72 ± 0.20	0.17 ± 0.04	0.08 ± 0.02
T2 / T1	1.14 ± 0.57	1.54 ± 0.53	0.62 ± 0.21	0.59 ± 0.20

References

Abdulla, H. A. N., Minor, E. C., Dias, R. F., and Hatcher, P. G.: Changes in the compound classes of dissolved organic matter along an estuarine transect: A study using FTIR and 13C NMR, Geochimica et Cosmochimica Acta, 74, 3815–3838, https://doi.org/10.1016/j.gca.2010.04.006, 2010.

Amoako, K., Reckhardt, A., Roberts, M., Meyer, R., Brick, S., Dittmar, T., and Waska, H.: Organo-mineral interactions modulate organic carbon retention and mobility in a deep subterranean estuary of a high-energy beach, Front. Water, 7, https://doi.org/10.3389/frwa.2025.1507564, 2025.

Artz, R. R. E., Chapman, S. J., Jean Robertson, A. H., Potts, J. M., Laggoun-Défarge, F., Gogo, S., Comont, L., Disnar, J.-R., and Francez, A.-J.: FTIR spectroscopy can be used as a screening tool for organic matter quality in regenerating cutover peatlands, Soil Biology and Biochemistry, 40, 515–527, https://doi.org/10.1016/j.soilbio.2007.09.019, 2008.

Božič, M., Elschner, T., Tkaučič, D., Bračič, M., Hribernik, S., Stana Kleinschek, K., and Kargl, R.: Effect of different surface active polysaccharide derivatives on the formation of ethyl cellulose particles by the emulsion-solvent evaporation method, Cellulose, 25, 6901–6922, https://doi.org/10.1007/s10570-018-2062-2, 2018.

Burdette, T. C., Bramblett, R. L., Deegan, A. M., Coffey, N. R., Wozniak, A. S., and Frossard, A. A.: Organic Signatures of Surfactants and Organic Molecules in Surface Microlayer and Subsurface Water of Delaware Bay, ACS Earth Space Chem., 6, 2929–2943, https://doi.org/10.1021/acsearthspacechem.2c00220, 2022.

Ji, Y., Yang, X., Ji, Z., Zhu, L., Ma, N., Chen, D., Jia, X., Tang, J., and Cao, Y.: DFT-Calculated IR Spectrum Amide I, II, and III Band Contributions of N -Methylacetamide Fine Components, ACS Omega, 5, 8572–8578, https://doi.org/10.1021/acsomega.9b04421, 2020.

Laurson, P., Raudsepp, P., Kaldmäe, H., Kikas, A., and Mäeorg, U.: The deconvolution of FTIR-ATR spectra to five Gaussians for detection of small changes in plant–water clusters, AIP Advances, 10, 085214, https://doi.org/10.1063/5.0011700, 2020.

Lechtenfeld, O. J., Koch, B. P., Gašparović, B., Frka, S., Witt, M., and Kattner, G.: The influence of salinity on the molecular and optical properties of surface microlayers in a karstic estuary, Marine Chemistry, 150, 25–38, https://doi.org/10.1016/j.marchem.2013.01.006, 2013.

Lu, R., Gan, W., Wu, B., Zhang, Z., Guo, Y., and Wang, H.: C−H Stretching Vibrations of Methyl, Methylene and Methine Groups at the Vapor/Alcohol (n = 1−8) Interfaces, J. Phys. Chem. B, 109, 14118–14129, https://doi.org/10.1021/jp051565q, 2005.

Minor, E. and Stephens, B.: Dissolved organic matter characteristics within the Lake Superior watershed, Organic Geochemistry, 39, 1489–1501, https://doi.org/10.1016/j.orggeochem.2008.08.001, 2008.

Pärnpuu, S., Astover, A., Tõnutare, T., Penu, P., and Kauer, K.: Soil organic matter qualification with FTIR spectroscopy under different soil types in Estonia, Geoderma Regional, 28, e00483, https://doi.org/10.1016/j.geodrs.2022.e00483, 2022.

Socrates, G.: Infrared and Raman Characteristic Group Frequencies: Tables and Charts, John Wiley & Sons, Chichester, 2001.